Fuel 203 (2017) 316–329

Contents lists available at ScienceDirect

Fuel

journal homepage: www.elsevier.com/locate/fuel

# Shock tube measurement and simulation of DME/*n*-butane/air mixtures: Effect of blending in the NTC region

Xue Jiang *, Zemin Tian, Yingjia Zhang, Zuohua Huang *

*State Key Laboratory of Multiphase Flow in Power Engineering, Xi'an Jiaotong University, Xi'an 710049, People's Republic of China*

## HIGHLIGHTS

- New ignition delay data of DME/*n*-butane/air mixtures were provided.
- Literature models were evaluated.
- The influences of DME addition on *n*-butane ignition were interpreted in the NTC region.

## ARTICLE INFO

*Article history:*
Received 31 January 2017
Received in revised form 19 April 2017
Accepted 26 April 2017

*Keywords:*
DME
*n*-Butane
Binary fuel
Ignition delay time
Chemical kinetic

## ABSTRACT

In this study, the ignition delay times of lean and stoichiometric DME/*n*-butane/air mixtures were measured behind reflected shock waves at pressures of 2 and 10 atm, temperatures from 650 to 1400 K. The performances of several chemical kinetic models were evaluated. Numerical simulation and chemical kinetic analysis were conducted in a broad temperature range and at various DME blending ratios to understand the interactions between DME and *n*-butane. It is found that DME addition can promote both the first-stage and overall ignition delay of *n*-butane in the NTC region.



## 1. Introduction

Nowadays, energy and environmental issues are becoming world matter of concern. People are searching for clean alternative fuel for vehicle and also paying particular attention to efficient combustion technology. Homogeneous charge compression ignition (HCCI) as a clean combustion mode is attracting growing concern in recent years. The HCCI is typically operated in fuel-lean conditions and based on the burning of homogeneous fuel mixtures. It is featured with the low temperature combustion, which can achieve high thermal efficiency and reduce the NOx and soot emissions simultaneously. The control of ignition timing is the major obstacle for the commercial application of HCCI engine. Previous studies indicate that the ignition of the HCCI combustion is mainly determined by the chemical kinetics of fuel [1,2]. Moreover, it is found that during the HCCI combustion, many hydrocarbon fuels are showing the two-stage heat release and the negative temperature coefficient (NTC) profile [3,4], the first-stage heat release is closely related to the low temperature kinetic [5,6]. It is proposed that by using the high octane number and high cetane number binary fuel mixture in the HCCI engine, the ignition timing can be well controlled and the engine operation region can be extended [5,6].

*n*-Butane/DME binary mixture is considered to be the ideal fuel for HCCI engine. *n*-Butane is the main ingredient of liquid petroleum gas, it is also a component of natural gas. The octane number of *n*-butane is close to that of gasoline. DME (Dimethyl Ether) is an oxygen-containing fuel, which has a high cetane number. Many previous studies were conducted on HCCI engines using the DME/*n*-butane fuel blends under various engine loads, fuel blending ratios and exhaust gas re-circulation (EGR) ratios, as gives in Ref. [7–10]. It is found that by varying the DME blending ratio, the ignition timing of HCCI engine can be adjusted; moreover, the engine operation region can be extended. Fundamentally, the ignition delay characteristics of both DME and *n*-butane have been widely studied. Specifically, for the neat DME, Pfahl et. al. [11] measured the ignition delay times of stoichiometric DME/air mixture in a shock tube at 13 and 40 atm from intermediate to low

* Corresponding authors.
*E-mail addresses:* xuejiang1128@xjtu.edu.cn (X. Jiang), zhhuang@xjtu.edu.cn (Z. Huang).

http://dx.doi.org/10.1016/j.fuel.2017.04.121
0016-2361/

temperatures (840–1300 K), they observed the NTC profile and two-stage auto-ignition behavior of DME experimentally. Then, Li et al. [12] followed up and measured the ignition delay of DME at the lean and rich condition in a shock tube, they also studied the effect of introducing nitrogen dilution gas. More recently, Cook et al. [13,14] measured the ignition delay times of argon diluted DME at temperatures of 1175–1900 K, pressures of 1.6–6.6 bar, and equivalence ratios of 0.5–3.0, they also measured the reaction rate of DME $\Leftrightarrow CH_3O + CH_3$. For the low-temperature ignition delay studies in the rapid compression machines (RCMs), Mittal and co-workers [15] measured the ignition delay times of DME/$O_2$/$N_2$ mixtures at pressures from 10 to 20 atm, temperatures from 615 K to 735 K and equivalence ratios from 0.43 to 1.5. They found that the NTC region of DME ignition is more significant at lower pressures, and the first-stage ignition delay is insensitive to pressure and equivalence ratio changes. More recently, Burke et al. [16] measured the ignition delay times of DME/methane mixtures at temperatures of 600–1600 K, pressures of 7–41 atm, and equivalence ratios of 0.3, 0.5, 1.0, and 2.0. They also developed a chemical kinetic model of DME, in which the pressure-dependent of the low-temperature oxidation reactions were considered. In addition, for the neat *n*-butane, Gersen et al. [17] measured the ignition delay times of *n*-butane/air and *iso*-butane/air using the RCM at temperatures of 660–1010 K, pressures of 14–36 atm and equivalence ratios of 0.5 and 1.0. Besides, Healy et al. [18–20] measured the ignition delay time of *n*-butane/air and *iso*-butane/air mixtures at equivalence ratios of 0.3–2.0, pressures up to 45 atm in both shock tube and RCM, they also developed a chemical kinetic model. Those studies show that, the NTC regime and two-stage ignition characteristics of *n*-butane and *iso*-butane can be captured in the low-temperature RCM measurements. The increase of pressure will lead to decreased ignition delay time of both the butane isomers and the reduced amplitude of the NTC region.

In practical applications, DME is used as a fuel additive and cetane number improver been blended with high octane number alkane fuels to enhance its ignition quality. The DME has high reactivity and will promote the generation of free radicals during the initial stage of combustion, which can strongly influence the HCCI combustion. Although many works have been conducted to study the ignition delays of neat DME and neat *n*-butane, the combustion mechanism of DME as additive blended with neat *n*-butane is still unclear, especially in the NTC region. Such information is necessary for understanding the ignition delay characteristic of binary fuel and the "knocking" problem in HCCI engines. Furthermore, the ignition delay data of binary fuels can be used as targets to develop and validate the kinetic models. The promoting effects of DME addition on methane ignition have been studied from low to high temperatures in Ref. [16,21,22], the nonlinear promoting effects of DME addition were observed, it is found that small amount of DME addition can obviously promote methane ignition. While the almost linear promoting effects of DME addition was found in the high temperature ignitions of propane and *n*-butane in Ref. [23–25]. Recently, Dames et al. [26] also observed the nonlinear promoting effect of DME addition on propane ignition in the low temperature NTC region.

To our knowledge, previous researches on the ignition delays of DME/*n*-butane blends were only conducted in the high temperature region, where the measured ignition delay times exhibit typical Arrhenius exponential dependence on the reciprocal temperatures; moreover, the fuel mixtures were diluted by 80% argon, as gives in Ref. [23,24,27]. It is found that at high temperatures and fuel-lean condition, the ignition delay times of DME and *n*-butane are quite close and fuel blending shows the negligible effects on ignitions. So far, the study of the ignition delay characteristic of DME/*n*-butane/air mixtures in the engine relevant NTC region has not yet been conducted. Therefore, in this study, both experiment and simulation analyses were carried out to interpret the kinetic coupling effects of DME addition on *n*-butane ignition delays. Different from previous studies, all the experiments were conducted using the fuel/air mixtures instead of the diluted ones, which are more comparable to the real engine conditions. Then, the measured ignition delay data were compared with the predictions of several chemical kinetic mechanisms. Again, the effect of DME addition on *n*-butane ignition delay in the NTC region, which is closely related to engine knocking problem, was clarified and the chemical kinetic of DME/*n*-butane binary fuel mixture was interpreted.

## 2. Experimental and numerical approach

### 2.1. Experimental setup

In this study, all the experiments were conducted in a shock tube device of the same construction and specification mentioned in our previous study [28]. In brief, the stainless-steel shock tube is separated by double PET (polyester terephthalate) diaphragms into a 4 m long driver section and a 5.3 m long driven section, the internal diameter of which is 11.5 cm. Four fast-response piezoelectric pressure transducers (PCB 113B26) together with three time interval counters (Fluke PM6690) were used to determine the incident shock velocity at the end-wall. Chemical equilibrium software Gaseq [29] was used to calculate the temperature and pressure behind the reflected shock wave. $CH^*$ chemiluminescence was selected by a narrow filter centered at 430 ± 10 nm and detected by a photomultiplier (Hamamatsu, CR131) located at the end-wall of the driven section. During the experiment, both $CH^*$ emission signal and pressure time history were recorded by a digital recorder (Yokogawa, DL750). Ignition delay time is defined as the time interval between the arrival of the incident shock wave at the end-wall and the extrapolation of the steepest rise of the end wall $CH^*$ chemiluminescence to the zero baseline, as shown in Fig. 1. All the test mixtures in this study were prepared in a 128 L stainless steel tank according to Dalton's law of partial pressure and allowed to settle 12 h to ensure sufficient mixing. A vacuum system (Nanguang 2ZX-30D rotary vane vacuum pump and ZJP-150 roots vacuum pump) was used to evacuate the shock tube and fuel tank. Before each measurement, the shock tube was evacuated below 1 Pa. Oxygen/nitrogen ($X_{O2}/X_{N2}$ = 21%/79%) mixtures were used to replace the real air. Detailed test mixture compositions are listed in Table 1. High-purity helium and nitrogen mixtures were used as driver gas. Purities of helium, oxygen and

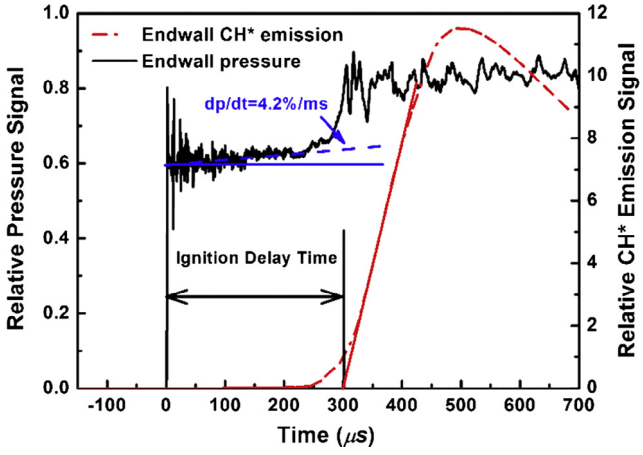


**Fig. 1.** Ignition delay time measurement from end-wall pressure and $CH^*$ emission.

**Table 1**
Composition of fuel mixtures.

| Mixtures | $\phi$ | $X_{DME}$ (%) | $X_{C4H10}$ (%) | $X_{O2}$ (%) | $X_{N2}$ (%) |
|---|---|---|---|---|---|
| 1.100%DME | 0.5 | 3.38 | 0.00 | 20.28 | 76.34 |
| 2. 50% DME/50% $C_4H_{10}$ | 0.5 | 1.08 | 1.08 | 20.52 | 77.32 |
| 3. 100%$C_4H_{10}$ | 0.5 | 0.00 | 1.59 | 20.67 | 77.74 |
| 4.100%DME | 1 | 6.54 | 0.00 | 19.62 | 73.84 |
| 5. 50% DME/50% $C_4H_{10}$ | 1 | 2.12 | 2.12 | 20.12 | 75.64 |
| 6. 100%$C_4H_{10}$ | 1 | 0.00 | 3.13 | 20.35 | 76.52 |

nitrogen used in this study are higher than 99.999%. The purity of DME and *n*-butane are 99.5% and 99.999% respectively.

The uncertainty of temperature behind the reflected shock wave was calculated according to standard root-sum-squares (RSS) method suggested by Petersen et al. [30], more detailed description of uncertainty analysis can be found in our previous study [31]. The largest uncertainty in the reflected temperature is estimated to be 20 K which will result in an uncertainty up to 20% in the measurement of ignition delay time.

### 2.2. Kinetic simulations

All simulations were conducted using SENKIN code [32] of CHEMKIN II program [33] with a zero-dimensional and constant volume adiabatic model. Non-ideal effects of the interaction between the boundary layer and reflected shock wave have been considered in simulations by using SENKIN/VTIM approach proposed by Chaos and Dryer [34]. An obvious pressure rise ($dp/dt$ = 4.2%/ms) [28] was observed experimentally and was taken into account in the numerical simulations. In the simulation, the first-stage and overall ignition delay times were determined according to the slope of the simulated OH time history.

For the DME/air mixture, four available chemical kinetic models were validated against the experimental data, namely Wang DME model [35], DME2000 model [36–38], San Diego DME model [39] and Aramco 2.0 model [40–46]. For the numerical simulations of *n*-butane/air mixtures, the Aramco2.0 model, the USC2.0 model [47] and San Diego 2016 model [48] were used.

**Wang DME model:** This mechanism consists of 56 chemical species and 301 elementary reactions. It was developed in 2015 based on the Zhao DME model [49] with updated low and intermediate temperature chemistry of DME oxidation.

**DME2000 model:** This mechanism is published by Lawrence Livermore National Laboratory, which includes 80 species and 351 reactions. It can be used to simulate both the low and high temperature oxidation of DME.

**San Diego DME model:** This is the skeletal model of DME oxidation, developed by the research group of UC San Diego in 2015. The model is based on the fourteen chemical-kinetic steps DME model developed by Prince et al. [50].

**Aramco2.0 model:** This mechanism is published by the combustion chemistry center of NUI Galway in 2016. The detailed mechanism consists of 493 species and 2716 reactions. It can be used to simulate the ignition and combustion behavior of C1-C4 based hydrocarbon and oxygenated fuels from low to high temperatures.

**USC2.0 model:** This is a high temperature combustion model suitable for $H_2$/CO/C1-C4 compounds which consist of 111 species and 784 reactions. The model is developed based on the GRI model [51], with updated sub-mechanisms of $H_2$/CO, ethylene, acetylene, 1, 3-butadiene and propene [52,53].

**San Diego 2016 model:** This mechanism is published by the combustion research group of UC San Diego in 2016, with newly added *n*-butane sub-mechanism based on the theoretical study by Prince et al. [54]. It includes the detailed chemistry of C0-C4 hydrocarbons and consists of 37 species and 269 reactions.

Fig. 2 (1), shows the comparisons between the measured and predicted ignition delay times of the DME/air at pressures of 2 and 10 atm, equivalence ratio of 0.5 and 1.0. Note that the San Diego DME model can only well reproduce the ignition delays of DME at high temperatures, while the predictions at low temperatures are obviously higher than the experimental data, as well as the predictions of other three models. Generally, the other three models, namely the Wang DME model, DME2000 model and Aramco 2.0 model, all give satisfactory predictions and agree well with the experimental data. At 10 atm and equivalence ratios of both 0.5 and 1.0, DME ignitions show obviously NTC behavior which can be easily seen from both experimental data and simulations.

Fig. 2 (2), shows the comparisons between the measured and model predicted ignition delay times of *n*-butane/air mixture. All the three models, namely, Aramco2.0 model, USC2.0 model and San Diego 2016 model, show moderately good predictions on *n*-butane ignition delay times in current conditions. The predictions of the San Diego 2016 model show the best agreements with the experimental data, while the predictions of the Aramco2.0 model are slightly slower than the San Diego 2016 model in the high temperature region. Meanwhile, the USC2.0 model is slightly faster than the San Diego2016 model at high temperatures, note that the USC2.0 model cannot capture the NTC behavior of *n*-butane at low temperature region, no surprise since this model only involves high temperature chemistry.

For 50%DME50%*n*-butane/air mixtures, as shown in Fig. 2 (3), the Aramco2.0 model which includes both DME and *n*-butane sub-mechanisms, present moderately good predictions for 50% DME50%*n*-butane/air binary mixture in current conditions.

The Aramco2.0 model was recently published in 2016 and the sub-mechanism of the butene isomers [40,41] and propene [43,44] were updated; these alkenes are important intermediates in the pyrolysis and oxidation of higher-order alkanes. In addition, the low and high temperature sub-mechanisms of the oxygenated fuels were also updated. This model has been widely validated against experimental data in the shock tubes, rapid compression machines, flames, jet-stirred and plug-flow reactors [40–46]. It is found that the model can well reproduce the ignition delay times of neat *n*-butane and *n*-butane/hydrocarbon mixtures [18,20,55] measured in the shock tube and RCM over a wide range of conditions. In addition, the DME sub-mechanism and related thermodynamic parameters of this model were based on the recent work of Burke et al. [16], which were also validated against a large number of experimental targets. As indicated in the previous research [26], the uncertainties in the low temperature oxidation of DME are largely related to the molecule oxygen addition reactions ($CH_3OCH_2 + O_2 \Leftrightarrow CH_3OCH_2O_2$ and $CH_2OCH_2O_2H + O_2 \Leftrightarrow O_2CH_2OCH_2O_2H$). Tomlin et al. [56] also pointed out the importance of these reactions and found some published DME models [45,57,58] cannot capture the low temperature ignition delay measurements in RCM [15]. Tomlin and co-workers [56], also emphasized the importance of considering the pressure-dependent of DME low temperature oxidation chemistry in the

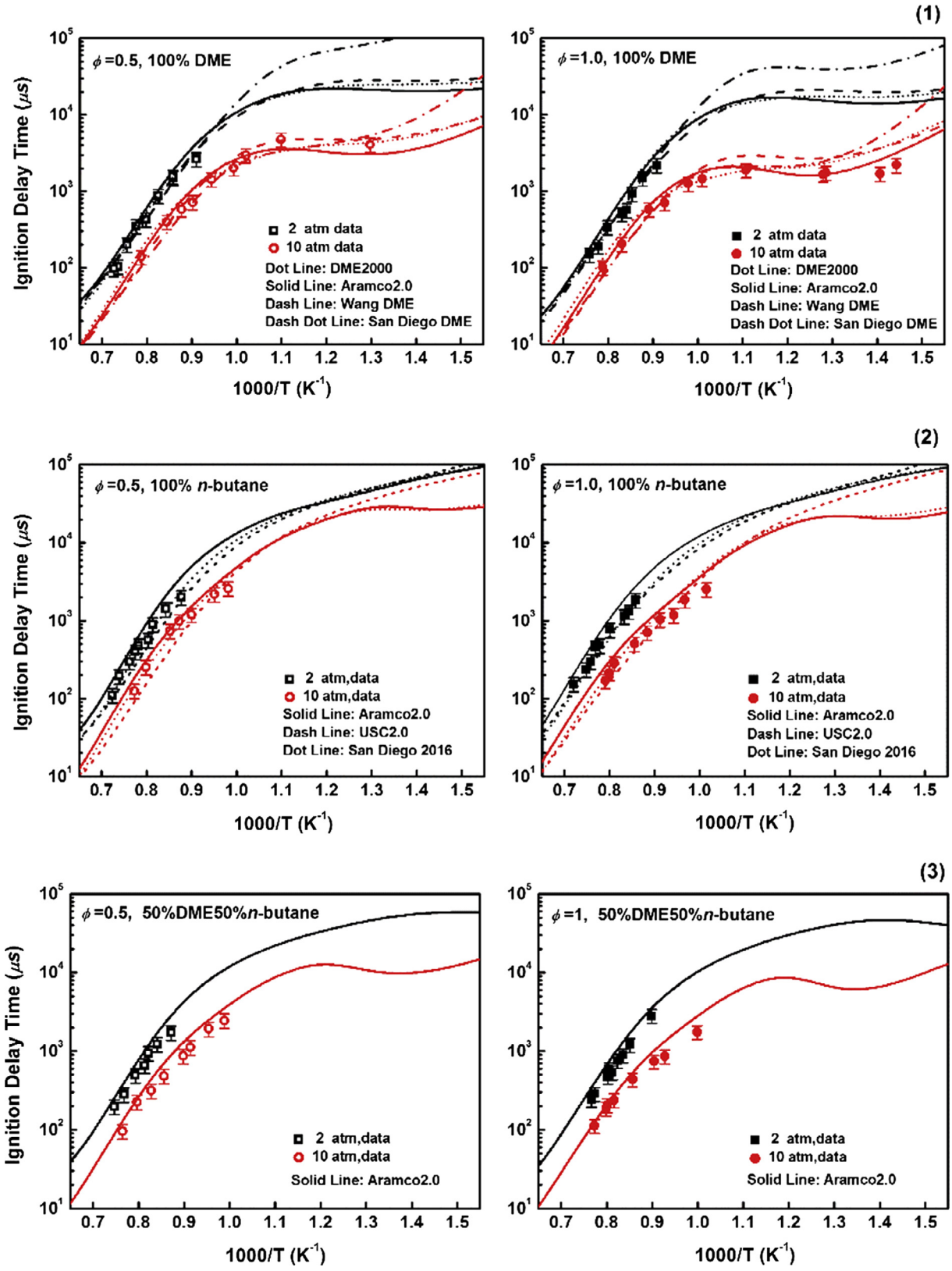


**Fig. 2.** Comparisons between the measured and model predicted ignition delay times using different mechanisms at pressures of 2 and 10 atm, equivalence ratios of 0.5 and 1.0.

development of the kinetic models. In the chemical kinetic model of Burke et al. [16], the Quantum-Rice-Ramsperger-Kassel calculations were conducted to acquire the pressure-dependent rates for the low-temperature oxidation of DME, including the first and second molecule oxygen addition reactions ($CH_3OCH_2 + O_2 \Leftrightarrow CH_3OCH_2O_2$ and $CH_2OCH_2O_2H + O_2 \Leftrightarrow O_2CH_2OCH_2O_2H$), the decomposition of

$CH_3OCH_2$, $CH_2OCH_2O_2H$ and $O_2CH_2OCH_2O_2H$, as well as the isomerization of $CH_3OCH_2O_2$.

Therefore, the Aramco2.0 model can well capture the ignition delay measurements in this study, moreover, the low temperature kinetics of this model have been recently updated. This model was used to calculate the ignition delay times and conduct the chemical kinetic analysis of the DME/*n*-butane/air fuel blends in this study.

## 3. Results and discussion

### 3.1. Ignition delay times and correlation

In this study, the ignition delay times of DME/*n*-butane/air mixtures were measured at pressures of 2 and 10 atm, temperatures of 650–1400 K and equivalence ratios of 0.5 and 1.0. All the experimental data can be seen in the Supporting Information. The experimental results show that, the ignition delay times of DME/air mixtures at both lean and stoichiometry conditions, exhibit the Arrhenius-type dependence only at high temperatures (T > 1000 K), besides, the NTC behavior of ignition delay was observed at intermediate and low temperatures. However, the *n*-butane/air and 50%DME50%*n*-butane/air mixtures give the typical Arrhenius-type dependence in all conditions, the NTC region of which cannot be reached experimentally due to the limitation of the current shock tube device. Basically, our shock tube can measure the ignition behavior at relatively high temperatures and pressure below 20 atm, where corresponds the longest ignition delay time of about 4 ms. However, the NTC characters of the *n*-butane/air and 50%DME50%*n*-butane/air can be acquired and have been analyzed in the chemical kinetic simulations.

The multiple linear regression method was used to obtain the Arrhenius-type correlation of ignition delay time. The correlations are used to estimate the dependence of fuel ignition delays on the equivalence ratio, pressure, temperature, dilution ratio et al. Those obtained global dependencies are helpful for understanding the fuel combustion chemistry. Moreover, the correlations were also conducted for comparative purposes, which provide the possibility to compare the measured ignition delay data with the literature data under different conditions, and between different facilities [59]. The basic form of the correlation is as follows:

$$\tau_{ign} = Ap^{\alpha}\phi^{\beta}Exp\left(\frac{E_a}{RT}\right) \quad (1)$$

where $\tau_{ign}$ is the ignition delay time in seconds, $p$ is the pressure in atmospheres, $\phi$ is the equivalence ratio, T is the temperature in kelvins, Ea is the activation energy in kilo calorie per mole, and $R = 1.986 \times 10^{-3}$ kcal mol$^{-1}$ K$^{-1}$ is the universal gas constant.

For DME/air mixture, the correlations were not applied in the temperatures below 1000 K, where corresponding to the NTC region and the ignition delay times no longer present the Arrhenius-type dependence on temperature. The correlation parameters of *n*-butane/air, DME/air and 50%DME/50%*n*-butane/air mixtures at equivalences of 0.5 and 1.0, pressures of 2 and 10 atm are given in Table 2, these correlation results can well reproduce the experimental measurement in current conditions.

### 3.2. Effect of pressure and equivalence ratio

Fig. 3 (1)–(3) give the effects of pressure and equivalence ratio on ignition delay times of DME/air, *n*-butane/air and 50%DME50% *n*-butane/air binary fuel. Note that for all mixtures, ignition delay times decreased with the increase of pressure, meaning that the increase of pressure can promote fuel ignition in current conditions. This is mostly due to the increased fuel concentration and enhanced molecule collision probability at elevated pressures.

The influences of equivalence ratio on the ignition delays of DME/air and *n*-butane/air mixtures were investigated at pressures of 2 and 10 atm. For the DME/air mixture, as shown in Fig. 3 (1), both experiment and simulation exhibit shorter ignition delay times under the fuel stoichiometric ($\phi = 1.0$) condition than the fuel lean ($\phi = 0.5$) condition from low to high temperatures, meaning that the ignition delay time of DME decreases with the increase of the equivalence ratio. For the *n*-butane/air mixture, as shown in Fig. 3 (2), the lean mixture ($\phi = 0.5$) ignite slightly faster than the stoichiometric mixture ($\phi = 1.0$) at high temperatures, however, with the decrease of temperature, the tendency becomes reversed and the fuel stoichiometric mixture exhibits shorter ignition delay time than the fuel lean mixture, especially in the NTC region. For the *n*-butane/air mixture at high temperatures, the reaction $O_2 + H \Leftrightarrow O + OH$ is the dominating chain-branching reaction [23], this indicates that the *n*-butane ignition is very sensitive to the oxygen concentration. Therefore, at high temperatures, the lean *n*-butane/air mixtures are more reactive and ignite faster than the stoichiometric mixtures. This is a common phenomenon for alkane fuels. For the 50% DME50% *n*-butane/air mixture, as shown in Fig. 3 (3), an ignition delay behavior similar to that of DME/air mixture is presented, an increasing equivalence ratio can promote the ignition and lead to shorter ignition delay times. It is also observed that, for the DME/air, *n*-butane/air and 50%DME50%*n*-butane/air mixtures, the influence of the equivalence ratio is less obvious in the high temperature region (T > 1000 K), however, becomes gradually stronger with the decrease of temperature.

### 3.3. Effect of DME addition

Previous researches [15,18] indicate that both the DME and *n*-butane are showing the NTC regime and two-stage heat release during their low temperature oxidation processes. DME has high reactive, the addition of which to the *n*-butane will promote the generation of free radicals at low temperatures during the initiation stage of ignition and enhance the reactivity. Fig. 4 shows the simulations of both the first-stage and overall ignition delay times of DME/*n*-butane/air mixtures at the equivalence ratio of 0.5, the pressure of 10 atm and various DME blending ratios. Note that in current condition, as DME blending ratio increases, both the first-stage and overall ignition delay of the fuel mixtures become shorter; meaning that both the first-stage and overall ignition delay can be promoted with the increase of the DME blending ratio. Fig. 5 illustrates the promoting effect of DME on *n*-butane ignition at the equivalence ratio of 0.5, temperatures of 700 K and 1200 K, the pressure of 10 atm and at various DME blending ratios. Apparently, the promoting effect of DME addition at 700 K is more significant than that at 1200 K. As illustrated in the figure,

**Table 2**
Correlation of DME/*n*-butane mixtures using Eq. (1).

| Mixture | A | $\alpha$ | $\beta$ | Ea (kcal/mol) | $R^2$ |
|---|---|---|---|---|---|
| 100% *n*-butane | $7.64 \times 10^{-3}$ | −0.613 | −0.103 | 29.01 ± 1.55 | 0.931 |
| 50%DME50%*n*-butane | $8.94 \times 10^{-3}$ | −0.625 | −0.230 | 28.19 ± 1.19 | 0.949 |
| 100%DME | $1.46 \times 10^{-3}$ | −0.672 | −0.387 | 31.90 ± 1.60 | 0.936 |

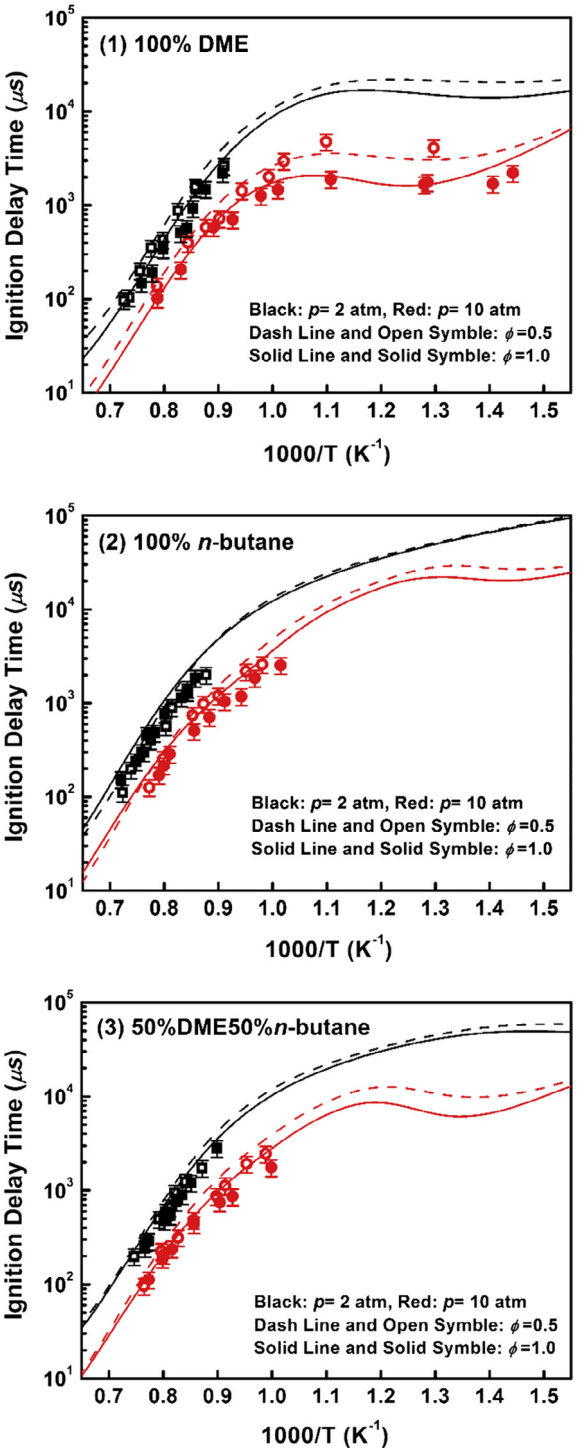


**Fig. 3.** Effect of pressure and equivalence ratio on ignition delay times of DME, *n*-butane and 50%DME50%*n*-butane blends at 2 and 10 atm. (Simulation: Aramco2.0 model).

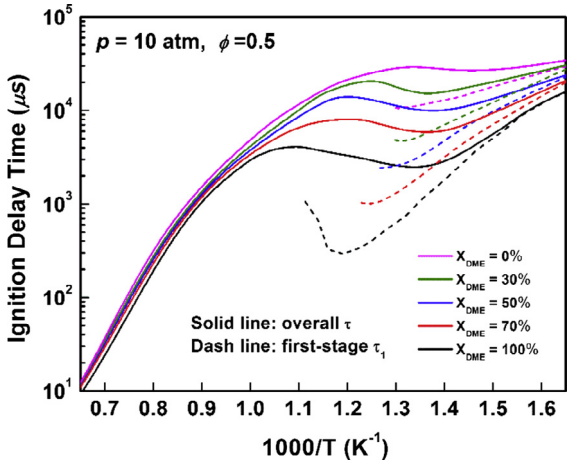


**Fig. 4.** Effect of DME addition on the first-stage and overall ignition delay times of *n*-butane at 10 atm and the equivalence ratio of 0.5. (Simulation: Aramco2.0 model).

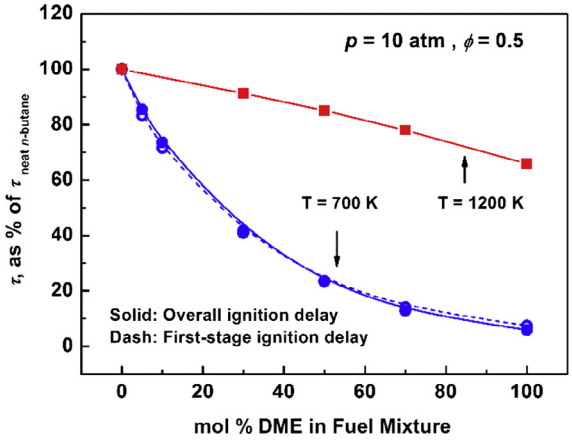


**Fig. 5.** Effect of DME addition on *n*-butane ignition delay times at 10 atm and the equivalence ratio of 0.5. (Simulation: Aramco2.0 model).

at 1200 K, DME addition gives an almost linear prompting effect on *n*-butane ignition, the 5% DME addition reduces the ignition delay time of *n*-butane by only 1.47%, while 30% DME addition can reduce the ignition delays of *n*-butane by 9.34% under current conditions. At high temperatures, it is found that only a small amount of DME addition can significantly promote the homogeneous ignition of methane [21,22]. However, the almost linear promoting effects of DME addition were found in propane and *n*-butane ignition delays [23,25]. This is mainly due to that the reactivity of methane is much lower relative to that of DME. Therefore, even with a small amount of DME addition, the ignition was strongly promoted by the decomposition of DME accompanied by the rapid build-up of free radicals, thus lead to the nonlinear promoting effect on methane ignition [21,22]. However, for the higher order alkanes, such as propane and butane, the reactivity of which are higher and the ignition delay times are much shorter relative to methane. Moreover, in the high temperature oxidation of methane, the rate of the governing reaction $CH_4 + O_2 \Leftrightarrow CH_3 + HO_2$ is much slower than of the similar reactions of the higher order alkanes [22]. Therefore, the nonlinear promoting of DME addition on ignition is not observed for higher order alkanes at high temperatures.

However, at 700 K, as shown in Fig. 5, with only 5% DME addition, the first stage and overall ignition delay times of *n*-butane were reduced by 16.71% and 14.57%, respectively. Such nonlinear promoting effect of DME addition in the low temperature ignition was also observed for methane and propane in Ref. [16,26]. Burke and co-workers [16] noticed the nonlinear promoting effect of DME addition on the overall ignition delay times of the 20% DME/80%methane mixture. Recently, Dames et al. [26] also found that with 5% DME addition, the ignition delay of propane was reduced by 20%. They pointed out that these nonlinear promoting effects at low temperatures are mainly due to the weaker C–H bonds of DME relative to those of methane and propane. In the cur-

rent study, the *n*-butane has longer carbon chain length, higher reactivity and weaker C–H bond, thus the nonlinear promoting effect of DME addition is less pronounced relative to propane and methane.

### 3.4. Chemical kinetic analysis

#### 3.4.1. Sensitivity analysis

Sensitivity analysis of DME/air and *n*-butane/air mixtures were performed at the pressure of 10 atm, equivalence ratios of 0.5 and 1.0, and the temperature of 700 K to find out the most important reactions that influence the ignition delay times in the NTC region. The top 10 most promoting and inhibiting reactions are shown in Fig. 6. The sensitivity coefficient is defined as,

$$S = \frac{\tau(2k_i) - \tau(k_i)}{\tau(k_i)} \quad (2)$$

where $\tau$ is ignition delay time, $k_i$ is the specific rate coefficient. A positive coefficient denotes that the reaction inhibits reactivity and vice versa.

At the temperature of 700 K, ignition delay times of the DME/air and *n*-butane/air mixture all decrease with the increase of equivalence ratio. Note that for both the DME/air and *n*-butane/air mixtures, the fuel radical species are playing the dominating role in the low temperature oxidation. These fuel radical species are directly produced from their parent fuel, therefore, the increased fuel concentration with the increase of equivalence ratio will lead to more pronounced chain branching of the fuel relevant radicals, thus promote the overall reactivity.

For both the lean and stoichiometric DME/air mixture at 700 K, as shown in Fig. 6, the sensitivity analyses indicate that the fuel relevant reactions: $CH_3OCH_2O + OH \Leftrightarrow CH_3OCH_2O_2H$ (R458), $CH_3OCH_2 + O_2 \Leftrightarrow CH_3OCH_2O_2$ (R446) and $CH_3OCH_3 + CH_3OCH_2O_2 \Leftrightarrow CH_3OCH_2 + CH_3OCH_2O_2H$ (R439) are the most-promoting reactions, which will finally lead to the low temperature chain-branching thus promote the reactivity. Meanwhile, the $\beta$- scission reaction of $CH_3OCH_2 \Leftrightarrow CH_3 + CH_2O$ (R445) is the most-inhibiting reaction, which yields $CH_3$ radical and $CH_2O$ and leads to a reduced reactivity.

Similarly, for the *n*-butane/air mixtures, in both lean and stoichiometric conditions, the H-atom abstractions of *n*-butane $C_4H_{10} + OH \Leftrightarrow PC_4H_9 + H_2O$ (R959) is the most promoting reaction, through which *n*-butyl radical ($PC_4H_9$) were produced. The $PC_4H_9$ radicals will lead to the increased production of the QOOH radicals and promote the low temperature chain branching. Another important ignition prompting reaction is the oxygen addition reaction $C_4H_8OOH2\text{-}4 + O_2 \Leftrightarrow C_4H_8OOH2\text{-}4O_2$ (R1115). The reactions $NC_4KET24 \Leftrightarrow CH_2O + CH_3COCH_2 + OH$ (R1164) and $NC_4KET13 \Leftrightarrow CH_3CHO + CH_2CHO + OH$ (R1168) are also considerably important, which will yield OH radical and promote the global reaction rate. It is interesting to notice that the secondary H-atom abstraction reaction of *n*-butane, $C_4H_{10} + OH \Leftrightarrow SC_4H_9 + H_2O$ (R981) is showing the obvious inhibiting effect on reactivity. This is because that the yield $SC_4H_9$ radicals will lead to the increased production of the butene isomers, which are the main ignition inhibiting channels during the low temperature ignition. Note that the reactions $PC_4H_9O_2 \Leftrightarrow C_4H_8\text{-}1 + HO_2$ (R1079) and $SC_4H_9O_2 \Leftrightarrow C_4H_8\text{-}1 + HO_2$ (R1042) are showing the high positive sensitivity coefficients that inhibiting fuel ignition at both equivalence ratios, both of which are chain propagation reactions and will cause a reduced reactivity.

#### 3.4.2. Reaction pathway analysis

In order to interpret the influence of DME addition on *n*-butane ignition, the reaction pathway of DME/air, *n*-butane/air and 50% DME/50% *n*-butane/air mixtures at both the first-stage ignition and the overall ignition were analyzed using the Aramco2.0 model at the equivalence ratio of 0.5, the temperature of 700 K and the pressure of 10 atm.

For the DME/air mixture during the first-stage ignition, as shown in Fig. 7, the DME molecule entirely undergoes H-atom abstraction reactions and yield methoxymethyl radical ($CH_3O\dot{C}H_2$), mostly by $\dot{O}H$ radical (94.5%) while the H radical (4.8%) also participated. Then, 77% of the $CH_3O\dot{C}H_2$ radicals combine with molecular oxygen and yield the methoxymethyl-peroxy radical ($CH_3OCH_2\dot{O}_2$) through the reaction $CH_3OCH_2 + O_2 \Leftrightarrow CH_3OCH_2O_2$. The rest of the $CH_3O\dot{C}H_2$ radical, accounting for 21.1%, proceeds $\beta$- scission or react with molecule oxygen to form the formaldehyde ($CH_2O$). After that, about 34.3% of the $CH_3OCH_2\dot{O}_2$ radical consumed through the reaction $CH_3OCH_2O_2 \Leftrightarrow 2CH_2O + OH$ and produced the $CH_2O$ and OH radical. Meanwhile, most of the unstable $CH_3OCH_2\dot{O}_2$ radical (64.7%) isomerizes via a 6-membered transition state ring to generate the hydroperoxy methoxymethyl radical ($\dot{C}H_2OCH_2O_2H$). Again, about 76.1% of the $\dot{C}H_2OCH_2O_2H$ radical proceed with $\beta$- scission, $CH_2OCH_2O_2H \Leftrightarrow 2CH_2O + OH$, while 23.3% of the generated $\dot{C}H_2OCH_2O_2H$ radical consumed by the molecular oxygen addition pathway yield the peroxy-hydroperoxyl-alkyl radicals ($\dot{O}_2CH_2OCH_2O_2H$). Again, all the produced $\dot{O}_2CH_2OCH_2O_2H$ radical releasing the OH radical and producing a carbonyl-hydroperoxide molecule, $HO_2CH_2OCHO$. The NTC behavior of DME ignition observed at low temperatures can be attributed to the competition between the branched pathways of $\beta$- scission and molecular oxygen addition reaction of the $CH_3O\dot{C}H_2$ radical and $\dot{C}H_2OCH_2O_2H$ radical [12], those chain propagation $\beta$- scission reactions will inhibit the reactivity, while the molecule oxygen addition pathway can lead to the low temperature chain branching to promote the ignition.

For the DME/air mixture at the overall ignition, which basically happens at high temperatures, the fuel molecules are entirely consumed through the H-atom abstraction by the OH (88.4%), O (8.3%) and H (3.2%) radicals, and formed the methoxymethyl radical ($CH_3OCH_2$). Subsequently, all the $CH_3OCH_2$ radical undergoes the $\beta$- scission and formed the $CH_3$ radical and formaldehyde ($CH_2O$).

For the *n*-butane/air mixture at the first-stage ignition, as shown in Fig. 7, the *n*-butane fuel molecule wholly undergoes primary (34%) and secondary (61.6%) H-atom abstraction reaction (mostly by $\dot{O}H$ radicals) and produces the *n*-butyl radical ($P\dot{C}_4H_9$) and the *sec*-butyl radical ($S\dot{C}_4H_9$), respectively. The proportion of the secondary H-atom abstraction is higher than the primary H-atom abstraction due to the lower bond dissociation energies of secondary hydrogen atoms. Then, nearly all the produced primary and secondary butyl radicals added to molecular oxygen, through reaction $PC_4H_9 + O_2 \Leftrightarrow PC_4H_9O_2$ (98.1%) and $SC_4H_9 + O_2 \Leftrightarrow SC_4H_9O_2$ (96%), and generate the *n*-butylperoxy radical ($PC_4H_9\dot{O}_2$) and the *sec*-butylperoxy radical ($SC_4H_9\dot{O}_2$) respectively. Most of the $PC_4H_9\dot{O}_2$ radicals then proceed H-atom isomerization through the reaction $PC_4H_9O_2 \Leftrightarrow C_4H_8OOH1\text{-}3$ (73.4%), $PC_4H_9O_2 \Leftrightarrow C_4H_8OOH1\text{-}4$ (8.4%), and $PC_4H_9O_2 \Leftrightarrow C_4H_8OOH1\text{-}2$ (1.8%), about 8% of the $PC_4H_9O_2$ radical also undergoes the molecular elimination channel to produce 1-butene through the reaction $PC4H_9O_2 \Leftrightarrow C_4H_8\text{-}1 + HO_2$. Similarly, about 24.5% of the $SC_4H_9\dot{O}_2$ radical undergoes isomerization to form the hydroperoxyl radicals, through the reactions $SC_4H_9O_2 \Leftrightarrow C_4H_8OOH2\text{-}3$ and $SC_4H_9O_2 \Leftrightarrow C_4H_8OOH2\text{-}4$. The yield $SC_4H_9\dot{O}_2$ radical also proceed the molecular elimination channel to produce butene isomers, $SC_4H_9O_2 \Leftrightarrow C_4H_8\text{-}1 + HO_2$ (26.8%), $SC_4H_9O_2 \Leftrightarrow C_4H_8\text{-}2 + HO_2$ (22.2%). A small amount of the $SC_4H_9\dot{O}_2$ radical (5.8%) also reacts with the $HO_2$ radical and yield the $SC_4H_9O_2H$. It is found that the NTC behavior on *n*-butane ignition is largely due to the branched pathways of the butylperoxy radicals, the generated hydroperoxy-butyl radicals will lead to low temperature chain-branching and ultimately

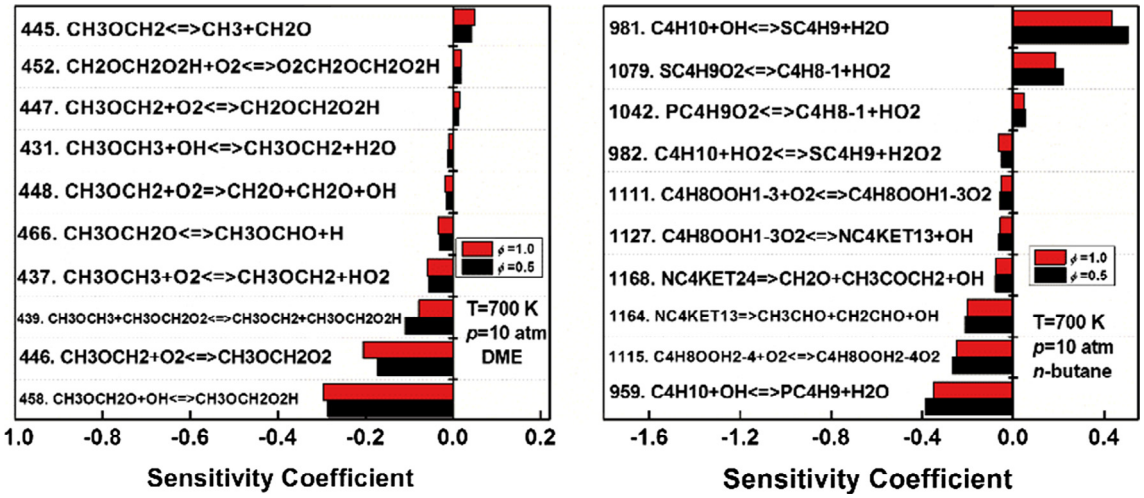


**Fig. 6.** Sensitivity analysis for DME/air and *n*-butane/air mixture at equivalence ratios of 0.5 and 1.0, the pressure of 10 atm and the temperature of 700 K. (Simulation: Aramco2.0 model).

promote the reactivity, however, the butene isomers will finally undergo chain propagation pathways and inhibit the ignition [18].

During the overall ignition of the *n*-butane/air mixture, most of the *n*-butane undergoes the H-atom abstraction reaction to produce the $SC_4H_9$ radical (26.3%) and $PC_4H_9$ radical (44.4%). The OH radical is playing the dominant role in *n*-butane H-atom abstraction, while O and OH radicals also participate. The vast majority of the $PC_4H_9$ radical undergo the $\beta$- scission to yield the ethyl radical ($C_2H_5$) and ethylene ($C_2H_4$). Meanwhile, 3.8% of the $SC_4H_9$ radical also formed the $C_4H_8$-1. At the same time, approximate 67.3% of the $SC_4H_9$ radical form the propene ($C_3H_6$) and $CH_3$ radical via $\beta$ – scission reactions. Meanwhile, 31.3% of the $SC_4H_9$ radical extract the H-atom and formed the butene isomers, $C_4H_8$-1 and $C_4H_8$-2. Besides the H-atom abstraction pathway, 10.7% of the *n*-butane also formed the propyl radical ($NC_3H_7$) and $CH_3$ radical through the C–C bond dissociation, while 18.6% of which also produces the $C_2H_5$ radical through the directed composition reaction.

For the 50%DME50%*n*-butane mixtures at the first-stage ignition, note that with *n*-butane addition, the molecular oxygen addition channel of the $CH_3O\dot{C}H_2$ radical obviously increased from 77% to 90.7%. In addition, the isomerization pathway of the $CH_3OCH_2\dot{O}_2$ radical that formed the $\dot{C}H_2OCH_2O_2H$ radical increased from 64.7% to 73.8%. Besides, 51.8% of the $\dot{C}H_2OCH_2O_2H$ radical proceed through the molecular oxygen addition pathway and yield the $\dot{O}_2$-$CH_2OCH_2O_2H$ radical, which is almost twice as much as that of the neat DME mixture. For the *n*-butane fuel, with the DME addition, the molecular oxygen addition of the $PC_4H_9$ radical reduced from 98.1% to 93.4% while that of the $SC_4H_9$ radical reduced from 96% to 88%. Note that more $SC_4H_9O$ radical and $PC_4H_9O$ radical were produced during the first-stage ignition. Generally, with *n*-butane addition, the low temperature oxidization pathway of DME was slightly enlarged during the first-stage ignition. At the same time, DME addition also leads to slightly reduced low temperature pathway of *n*-butane in the first-stage ignition.

### 3.4.3. First-stage heat release, temperature and fuel consumption

The previous study indicates that [5], the temperature increase in the initial stage of ignition can dramatically influence the fuel ignition delay time since the ignition chemistry is largely driven by the temperature changes during the oxidation process. It is also found that in the current study, fuel blending will affect the system temperature during the first-stage ignition, which will also influence the reaction pathways.

Fig. 8 shows the simulated net heat release and temperature time histories of the DME/air, *n*-butane/air and 50%DME50%*n*-butane/air mixtures at the initial temperature of 700 K, the pressure of 10 atm, and the equivalence ratio of 0.5. As shown in figure, all the mixtures show obviously two-stage temperature increases. For the DME/air mixture, as gives in Fig. 8 (1), an intense first-stage heat release was observed and accompanied by the rapid temperature increase during the first-stage ignition. With 50% *n*-butane addition, as gives in Fig. 8 (2), the first-stage temperature increase becomes more gentle; meanwhile, the heat release significantly reduced. Note that for the *n*-butane/air mixture, shown in Fig. 8 (3), the first-stage heat release is not obvious. The simulation also shows that under the same initial temperature of 700 K, the first-stage ignition temperature of the DME/air mixture is 874 K; while that for the 50%DME/50%*n*-butane mixture is 793 K. For the *n*-butane/air mixture, however, the temperature only increased from 700 K to 757 K during the first-stage ignition. Consequently, the heat release during the first-stage ignition will affect the system temperature; therefore influence the reaction pathway and the ignition kinetics.

From the practical application point of view, it is necessary to understand the influence of DME addition on temperatures during the first-stage ignition in the NTC region. Fig. 9 shows the calculations of the first-stage temperature increment of $X_{DME}$ = 0%, 30%, 50%, 70% and 100% mixtures at 10 atm and the equivalence ratio of 0.5. The first-stage temperature increment is defined as the temperature difference between the initial temperature and the first-stage ignition temperature. Firstly, for the given mixture, the first-stage temperature increment reduces with the increase of initial temperature, similar observation has been found in the experimental measurement of *n*-heptane in Ref. [60]. Secondly, the DME/air mixture gives the highest first-stage temperature increment, while the *n*-butane/air mixture shows the lowest one. This is because that the DME mixture releases more heat during the first stage ignition relative to the *n*-butane, as indicated in Fig. 8. Thirdly, at the given temperature of 700 K, as the DME mole fraction varies from 0% to 100%, the first-stage temperature increment also increases with the increasing DME blending ratio, meaning that the first-stage ignition temperature will increase with the increase of DME blending ratio.

Fig. 10 shows the simulated overall fuel consumption in the first-stage ignition of $X_{DME}$ = 0%, 30%, 50%, 70% and 100% mixtures at 10 atm and the equivalence ratio of 0.5. Note that, for all fuel mixtures, the fraction of fuel consumption in the first-stage

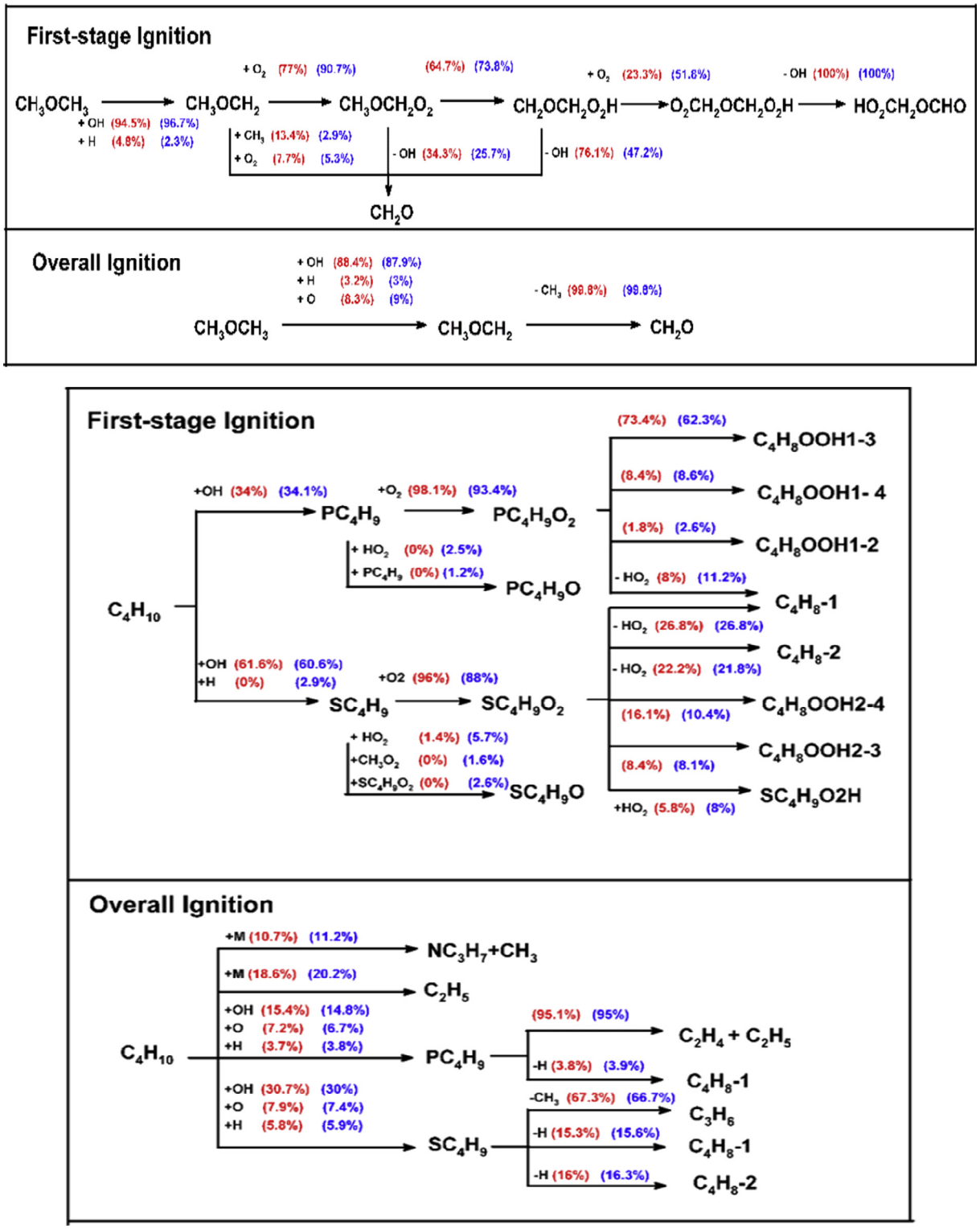


**Fig. 7.** Reaction pathway of DME/air, *n*-butane/air and 50%DME50%*n*-butane/air mixture at first-stage ignition and overall ignition, at the pressure of 10 atm, the temperature of 700 K, and the equivalence ratio of 0.5. (Red: 100% DME/air or 100% *n*-butane/air mixture; Blue: 50%DME50%*n*-butane/air mixture. Simulation: Aramco2.0 model). (For interpretation of the references to colour in this figure legend, the reader is referred to the web version of this article.)

ignition decreases with the increasing temperature, similar observation was also noticed in *n*-heptane oxidation in Ref. [60,61]. As obtained from the simulations, in all temperatures, the first-stage fuel consumption of *n*-butane/air mixture is the lowest; however, that of the DME/air mixture is the highest, DME addition can increase the fuel consumption during the first-stage ignition. Specifically, at the given temperature of 700 K, the fuel consumption fraction in the first-stage ignition shows a gradual growth with the increment of DME blending ratio. As discussed above, DME can release more heat during the first-stage ignition relative

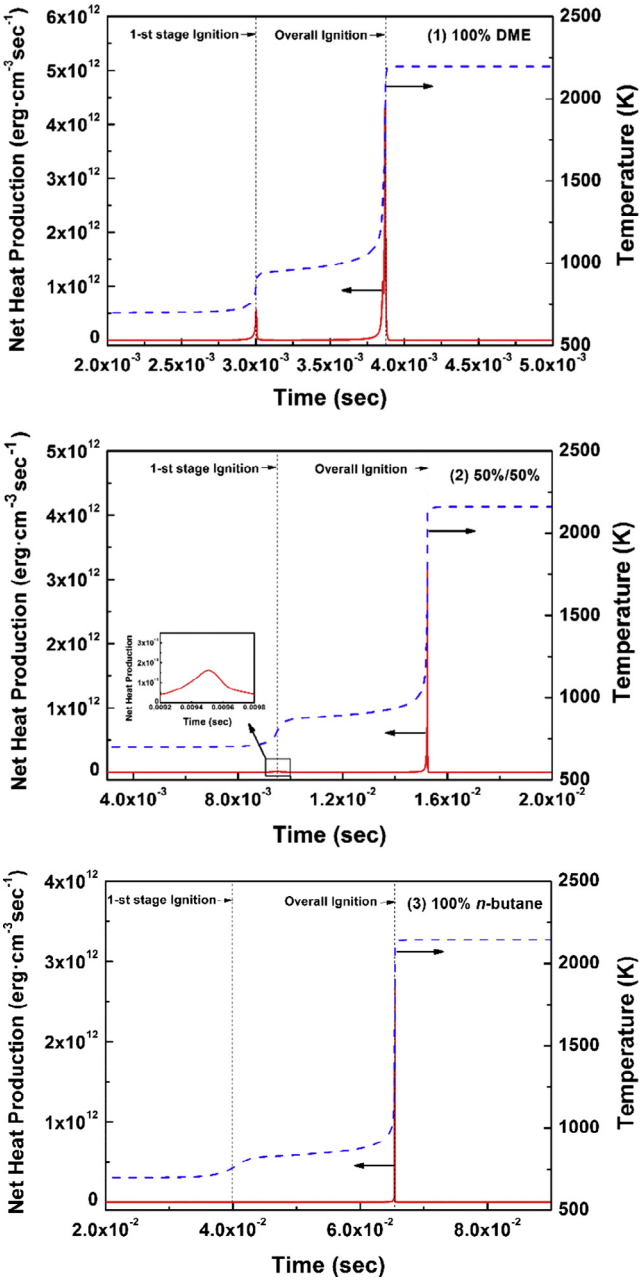


**Fig. 8.** Net heat release and temperature time-histories of 100% DME, 100% *n*-butane and 50%DME50%*n*-butane mixtures at the initial temperature of 700 K, the pressure of 10 atm, and the equivalence ratio of 0.5. (Simulation: Aramco2.0 model).

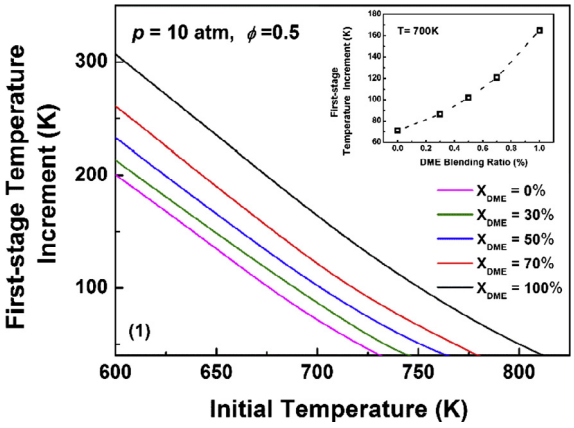


**Fig. 9.** Calculations of the first-stage temperature increment of $X_{DME}$ = 0%, 30%, 50%, 70% and 100% mixtures at 10 atm and the equivalence ratio of 0.5. (Simulation: Aramco2.0 model).

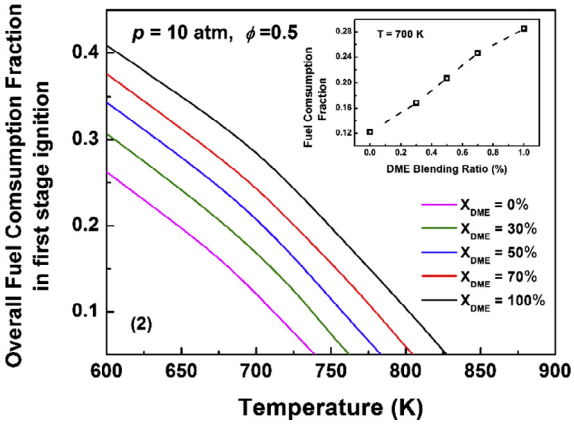


**Fig. 10.** The overall fuel consumption in the first-stage ignition of $X_{DME}$ = 0%, 30%, 50%, 70% and 100% mixtures at 10 atm and the equivalence ratio of 0.5. (Simulation: Aramco2.0 model).

to neat *n*-butane. This will lead to the increased temperature, thus more fuels are consumed during the first-stage ignition and the ignition of *n*-butane can be promoted.

### 3.4.4. Mole fraction and ROP analysis

As indicated in the reaction pathway analysis, the OH radical is playing an important role in the chain initiation of both DME and *n*-butane under current condition. Moreover, in the low temperature chemistry of DME and *n*-butane, the fuel relevant radical species, namely the R radical and $RO_2$ radical, are also dominating the low temperature chain branching. To identify the inter-reactions between DME and *n*-butane at low temperature during the first stage ignition, the simulated species profiles of the OH radical, R radical (including $CH_3OCH_2$, $PC_4H_9$ and $SC_4H_9$) and $RO_2$ radical (including $CH_3OCH_2O_2$, $PC_4H_9O_2$ and $SC_4H_9O_2$), as well as the rate of production and consumption (ROP) analysis of these radicals for the DME/air, *n*-butane/air and the 50%DME/50% *n*-butane/air binary mixture are presented in Figs. 11–14. All the simulations were conducted using the Aramco2.0 model at the temperature of 700 K, the pressure of 10 atm, and the equivalence ratio of 0.5, which corresponding to the NTC region.

The OH radical mole fraction profile of the DME/air, *n*-butane/air and 50%DME50%*n*-butane/air mixtures is shown in Fig. 11 (1). During the first stage ignition, the OH radical concentration slightly increased, while most of the OH radicals were generated at high temperatures during the overall ignition. For the R radical, as gives in Fig. 11 (2), evident two-stage mole fraction profile was observed with the increasing temperature. In addition, as shown in Fig. 11 (3), it is found that the concentration peak of the $RO_2$ radical appears during the first stage ignition. Generally, the simulation results demonstrate that the OH, R and $RO_2$ radicals are more quickly formed during the ignition induction time of DME compared to that of *n*-butane. The DME addition will lead the increase of mole fractions of OH, R and $RO_2$ radicals, which will increase the reactivity and decrease the ignition delay.

Rates of production and consumption the OH, R and $RO_2$ radicals during the first stage ignition are given in Figs. 12–14. Simulation results show that for the DME/air mixture in the first-stage ignition, Fig. 12 (1), the OH radicals are mainly produced from

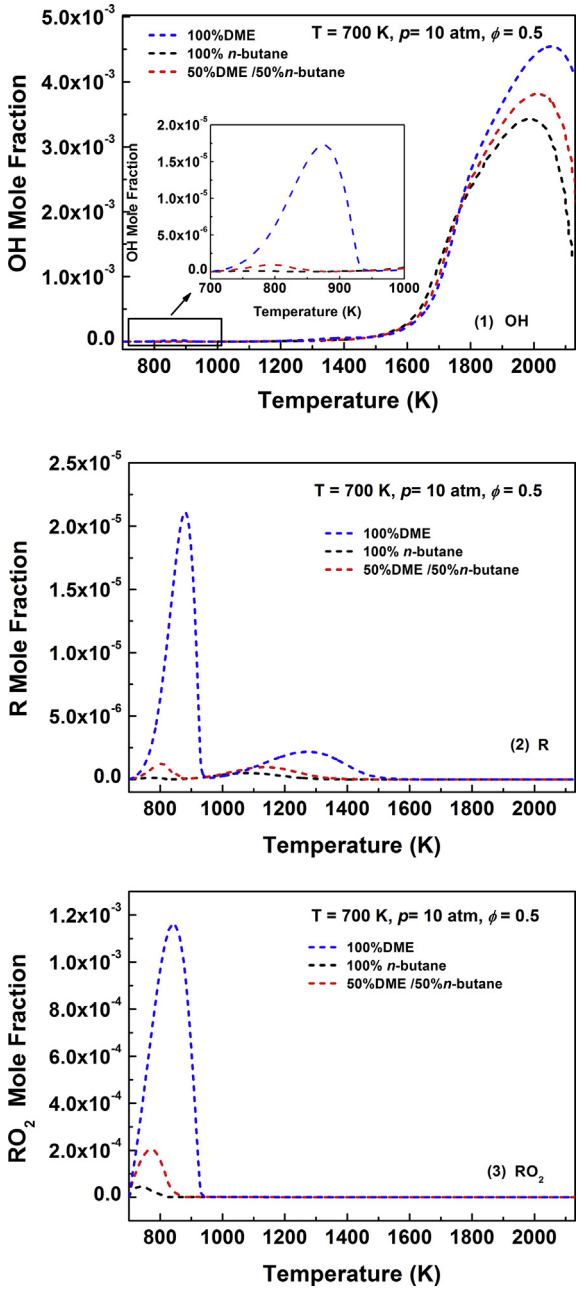


**Fig. 11.** Effect of DME addition on the mole fractions of OH radical, R radical (including $CH_3OCH_2$, $PC_4H_9$ and $SC_4H_9$) and $RO_2$ radical (including $CH_3OCH_2O_2$, $PC_4H_9O_2$ and $SC_4H_9O_2$) at the temperature of 700 K, the pressure of 10 atm, and the equivalence ratio of 0.5. (Simulation: Aramco2.0 model).

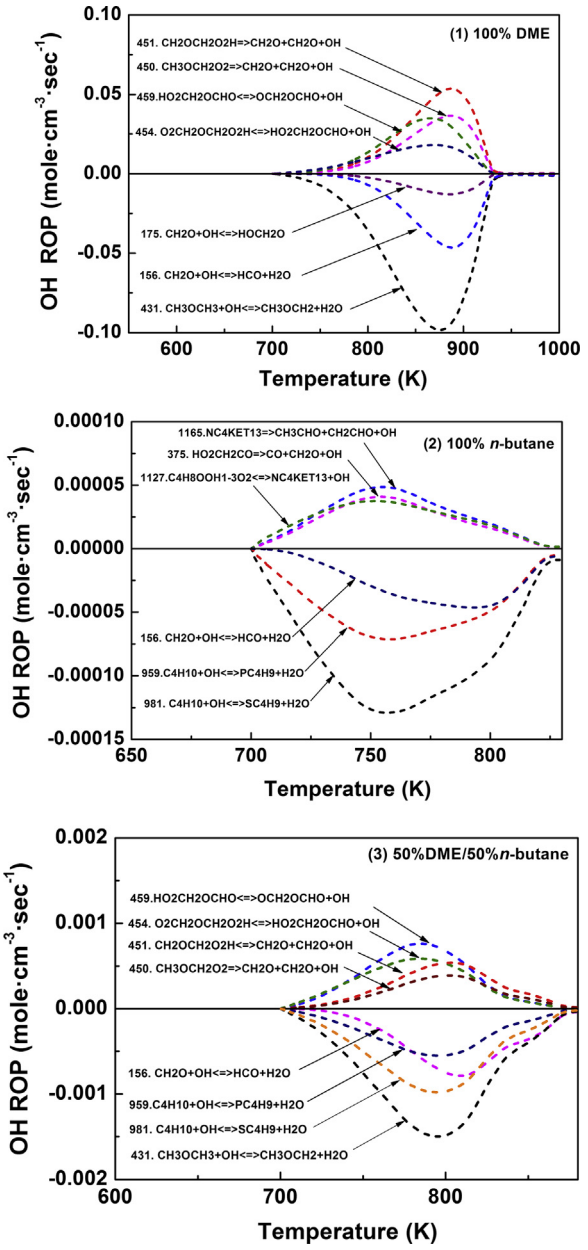


**Fig. 12.** Rates of production and consumption of the OH radical for 100% DME, 100% *n*-butane and 50%DME50%*n*-butane mixtures at T = 700 K, $p$ = 10 atm and $\phi$ = 0.5. (Simulation: Aramco2.0 model).

the following fuel radical species relevant reactions, $CH_3OCH_2O_2$ - ⇔ $CH_2O + CH_2O + OH$ (R450), $CH_2OCH_2O_2H \Leftrightarrow CH_2O + CH_2O + OH$ (R451), $O_2CH_2OCH_2O_2H \Leftrightarrow HO_2CH_2OCHO + OH$ (R454) and $HO_2CH_2OCHO \Leftrightarrow OCH_2OCHO + OH$ (R459). Meanwhile, the OH radicals are mostly consumed by the DME molecule through H-atom abstraction reaction, $CH_3OCH_3 + OH \Leftrightarrow CH_3OCH_2 + H_2O$ (R431).

For the *n*-butane/air mixture in the first-stage ignition, Fig. 12 (2), however, the OH radicals are mainly produced from the following reactions, $HO_2CH_2CO \Leftrightarrow CO + CH_2O + OH$ (R375), $C_4H_8OOH1-3O_2 \Leftrightarrow NC_4KET13 + OH$ (R1127) and $NC_4KET13 \Leftrightarrow CH_3CHO + CH_2CHO + OH$ (R1165). Note that the production rate of the OH radical of the *n*-butane/air mixture is significantly lower relative to the DME/air mixture. This will lead to the decreased reactivity and longer ignition delay time. It is also found that for the *n*-butane/air mixture, most of the OH radicals are consumed through the *n*-butane molecule H-atom abstractions during the first stage ignition, $C_4H_{10} + OH \Leftrightarrow SC_4H_9 + H_2O$ (R981) and $C_4H_{10} + OH \Leftrightarrow PC_4H_9 + H_2O$ (R959).

For the 50%DME/50%*n*-butane/air mixture, as shown in Fig. 12 (3), similar to the DME/air mixture, most of the OH radicals are generated by the DME fuel radical species relevant reactions (R450), (R451), (R454) and (R459). The contribution of the *n*-butane relevant reactions to the OH radical growth during the first-stage ignition is limited. Note that with DME addition, the production rate of the OH radical obviously increased relative to the *n*-butane/air mixture. As a result, DME addition can increase the OH radical production during the first-stage ignition, thus promote the ignition of *n*-butane in current condition. Note that the produced OH radical are mainly consumed by the fuel molecule H-atom abstraction reactions of both DME and *n*-butane.

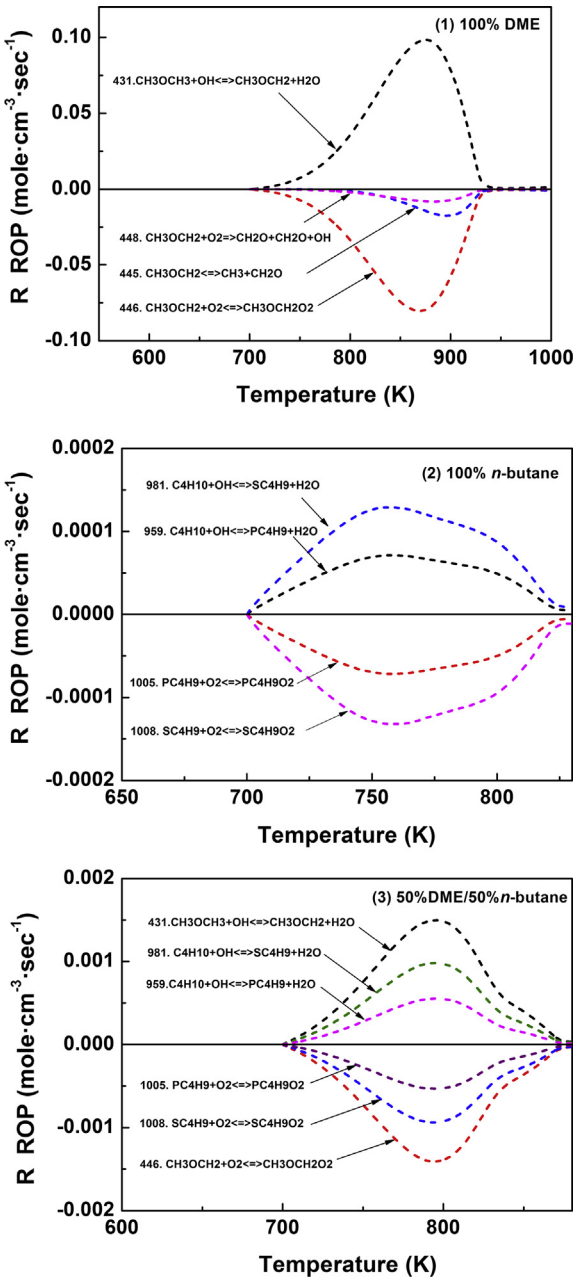


**Fig. 13.** Rates of production and consumption of the R radical for 100% DME, 100% *n*-butane and 50%DME50%*n*-butane mixtures at T = 700 K, $p$ = 10 atm and $\phi$ = 0.5. (Simulation: Aramco2.0 model).

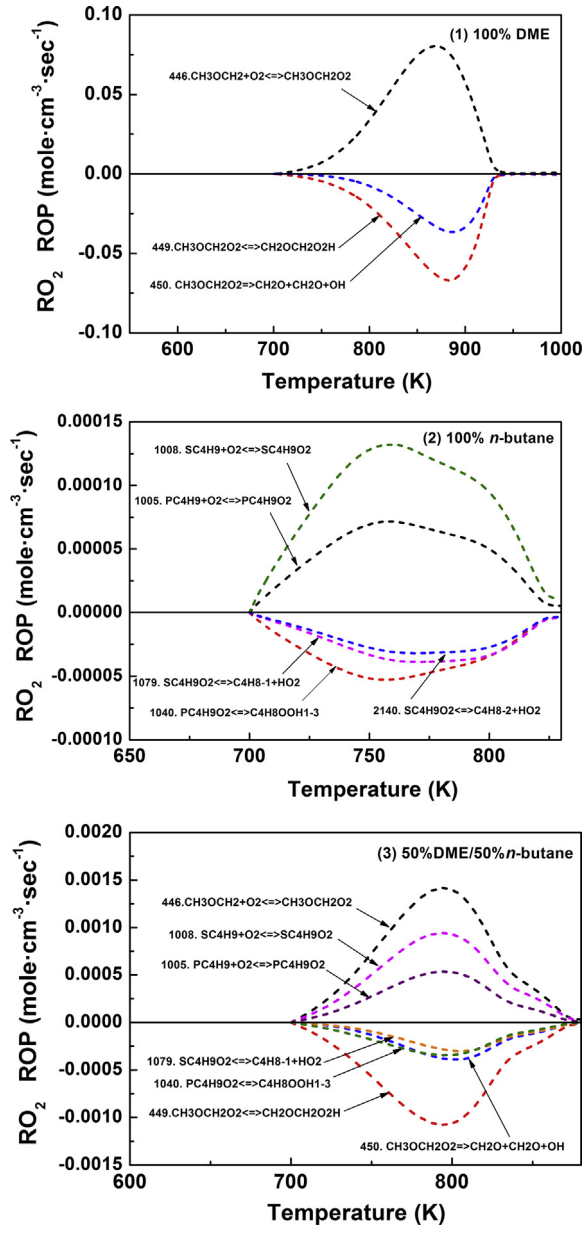


**Fig. 14.** Rates of production and consumption of the $RO_2$ radical for 100% DME, 100% *n*-butane and 50%DME50%*n*-butane mixtures at T = 700 K, $p$ = 10 atm and $\phi$ = 0.5. (Simulation: Aramco2.0 model).

Fig. 13 shows ROP analysis of the R radical during the first stage ignition. For the DME/air mixture, Fig. 13 (1), it is found that the reaction $CH_3OCH_3 + OH \Leftrightarrow CH_3OCH_2 + H_2O$ (R431) is the key reaction to produce the R radical, and the reaction $CH_3OCH_2 + O_2 \Leftrightarrow CH_3OCH_2O_2$ (R446) is the key reaction consuming it. For the *n*-butane/air mixture, Fig. 13 (2), the reaction $C_4H_{10} + OH \Leftrightarrow SC_4H_9 + H_2O$ (R981) and $C_4H_{10} + OH \Leftrightarrow PC_4H_9 + H_2O$ (R959) give the greatest contribution to the R radical formation, while the generated R radical are mainly consumed through the molecule oxygen addition reactions of $PC_4H_9 + O_2 \Leftrightarrow PC_4H_9O_2$ (R1005) and $SC_4H_9 + O_2 \Leftrightarrow SC_4H_9O_2$ (R1008). For the 50% DME/50% *n*-butane/air mixture, Fig. 13 (3), a combined ROP profile of both the DME/air mixture and *n*-butane/air mixture was observed. The R radicals are formed from both the DME and *n*-butane fuel molecule through reactions (R431), (R981) and (R959); while mainly consumed by the reactions (R446), (R1005) and (R1008).

Similarly, the ROP analysis of the $RO_2$ radical shows that, as gives in Fig. 14 (1)–(3), for the DME/air mixture and *n*-butane/air mixtures, the $RO_2$ radicals are mainly formed by the reaction (R446), (R1005) and (R1008), respectively. For the DME/air mixture, the yield $CH_3OCH_2O_2$ radicals then consumed by $CH_3OCH_2O_2 \Leftrightarrow CH_2OCH_2O_2H$ (R449) and $CH_3OCH_2O_2 \Leftrightarrow CH_2O + CH_2O + OH$ (R450). For the *n*-butane/air mixture, those $RO_2$ radicals were then consumed through the reactions, $PC_4H_9O_2 \Leftrightarrow C_4H_8OOH1\text{-}3$ (R1040), $SC_4H_9O_2 \Leftrightarrow C_4H_8\text{-}1 + HO_2$ (R1079) and $SC_4H_9O_2 \Leftrightarrow C_4H_8\text{-}2 + HO_2$ (R2140). The 50%DME/50%*n*-butane/air mixture also shows a combined production and consumption profile of both DME and *n*-butane mixtures. Generally speaking, with DME addition, the rates of production of both R and $RO_2$ radical are increased

relative to that of *n*-butane/air, which leads to the enhanced system reactivity and decreased ignition delay times.

## 4. Conclusions

Ignition delay times of DME/air, *n*-butane/air and 50%DME50% *n*-butane/air mixtures were measured in a shock tube at equivalence ratios of 0.5 and 1.0 and pressures of 2 and 10 atm. The chemical kinetic study was conducted using the Aramco2.0 model. The main conclusions are as follows:

(1) Ignition delay times of DME/air, *n*-butane/air and 50% DME50%*n*-butane/air mixtures were measured. Arrhenius type correlations of ignition delay times were obtained by using multiple linear regression analysis.
(2) The measured ignition delay times were compared with numerical predictions from six available mechanisms, namely Aramco2.0 model, Wang DME model, DME2000 model, San Diego DME model, USC2.0 model and San Diego 2016 model. The Aramco2.0 model gives satisfactory predictions on ignition delay times of both neat and binary fuels, therefore been adopted in the chemical kinetic analysis in this study.
(3) It is found that the increase of pressure can promote the ignition of DME/air, *n*-butane/air and DME/*n*-butane/air binary fuel mixture. For the DME/air mixture, ignition delay time decreases with the increase of the equivalence ratio. However, for the *n*-butane/air mixture, the lean mixture ignites slightly faster than the stoichiometric mixture at high temperatures; this tendency becomes reversed with the decrease of temperature. For the 50%DME50%*n*-butane/air mixture, the ignition behavior is similar to that of the DME/air mixture.
(4) It is found that DME addition can promote both the first-stage and overall ignition delays of *n*-butane in the NTC region. Simulations indicate that DME addition can promote the first-stage heat release, thereby increase the first-stage ignition temperature and the first-stage fuel consumption. It is also found that DME addition can accelerate the formation the OH, R and $RO_2$ radicals in the first stage ignition of *n*-butane.

## Acknowledgments

This work is supported by National Natural Science Foundation of China [51506164 and 91441203] and China Postdoctoral Science Foundation [2015M570831].

## Appendix A. Supplementary data

Supplementary data associated with this article can be found, in the online version, at http://dx.doi.org/10.1016/j.fuel.2017.04.121.

## References

[1] Stanglmaier RH, Roberts CE. Homogeneous charge compression ignition (HCCI): benefits, compromises, and future engine applications: SAE Technical Paper; 1999. Report No.: 0148-7191.
[2] Aceves SM, Flowers DL, Westbrook CK, Smith JR, Pitz W, Dibble R, et al. A multi-zone model for prediction of HCCI combustion and emissions: SAE Technical paper; 2000. Report No.: 0148-7191.
[3] Westbrook CK. Chemical kinetics of hydrocarbon ignition in practical combustion systems. Proc Combust Inst 2000;28(2):1563–77.
[4] Curran HJ, Gaffuri P, Pitz WJ, Westbrook CK. A comprehensive modeling study of n-heptane oxidation. Combust Flame 1998;114(1):149–77.
[5] Tanaka S, Ayala F, Keck JC, Heywood JB. Two-stage ignition in HCCI combustion and HCCI control by fuels and additives. Combust Flame 2003;132(1):219–39.
[6] Kaimai T, Tsunemoto H, Ishitani H. Effects of a hybrid fuel system with diesel and premixed DME/methane charge on exhaust emissions in a small DI diesel engine: SAE Technical Paper; 1999. Report No.: 0148-7191.
[7] Oh C, Jang J, Bae C. The effect of LPG composition on combustion and performance in a DME-LPG dual-fuel HCCI engine: SAE Technical Paper; 2010. Report No.: 0148-7191.
[8] Yeom K, Bae C. Knock characteristics in liquefied petroleum gas (LPG)–dimethyl ether (DME) and gasoline– DME homogeneous charge compression ignition engines. Energy Fuel 2009;23(4):1956–64.
[9] Song R, Li K, Feng Y, Liu S. Performance and emission characteristics of DME engine with high ratio of EGR. Energy Fuel 2009;23(11):5460–6.
[10] Igarashi T, Iida N. Auto ignition and combustion of DME and n-butane/air mixtures in Homogeneous Charge Compression Ignition engine. Nihon Kikai Gakkai Ronbunshu, B Hen/Trans Japan Soc Mech Eng, Part B 1998;64 (618):605–12.
[11] Pfahl U, Fieweger K, Adomeit G. Self-ignition of diesel-relevant hydrocarbon-air mixtures under engine conditions. In: Symposium (international) on combustion. Elsevier; 1996. p. 781–9.
[12] Li Z, Wang W, Huang Z, Oehlschlaeger MA. Dimethyl ether autoignition at engine-relevant conditions. Energy Fuel 2013;27(5):2811–7.
[13] Cook RD, Davidson DF, Hanson RK. Shock tube measurements of ignition delay times and OH time-histories in dimethyl ether oxidation. Proc Combust Inst 2009;32(1):189–96.
[14] Cook RD, Davidson DF, Hanson RK. High-temperature shock tube measurements of dimethyl ether decomposition and the reaction of dimethyl ether with OH. J Phys Chem A 2009;113(37):9974–80.
[15] Mittal G, Chaos M, Sung C, Dryer FL. Dimethyl ether autoignition in a rapid compression machine: experiments and chemical kinetic modeling. Fuel Process Technol 2008;89(12):1244–54.
[16] Burke U, Somers KP, O Toole P, Zinner CM, Marquet N, Bourque G, et al. An ignition delay and kinetic modeling study of methane, dimethyl ether, and their mixtures at high pressures. Combust Flame 2015;162(2):315–30.
[17] Gersen S, Mokhov AV, Darmeveil JH, Levinsky HB. Ignition properties of n-butane and iso-butane in a rapid compression machine. Combust Flame 2010;157(2):240–5.
[18] Healy D, Donato NS, Aul CJ, Petersen EL, Zinner CM, Bourque G, et al. n-Butane: ignition delay measurements at high pressure and detailed chemical kinetic simulations. Combust Flame 2010;157(8):1526–39.
[19] Healy D, Donato NS, Aul CJ, Petersen EL, Zinner CM, Bourque G, et al. Isobutane ignition delay time measurements at high pressure and detailed chemical kinetic simulations. Combust Flame 2010;157(8):1540–51.
[20] Healy D, Kopp MM, Polley NL, Petersen EL, Bourque G, Curran HJ. Methane/n-butane ignition delay measurements at high pressure and detailed chemical kinetic simulations. Energy Fuel 2010;24(3):1617–27.
[21] Tang C, Wei L, Zhang J, Man X, Huang Z. Shock tube measurements and kinetic investigation on the ignition delay times of methane/dimethyl ether mixtures. Energy Fuel 2012;26(11):6720–8.
[22] Chen Z, Qin X, Ju Y, Zhao Z, Chaos M, Dryer FL. High temperature ignition and combustion enhancement by dimethyl ether addition to methane–air mixtures. Proc Combust Inst 2007;31(1):1215–22.
[23] Jiang X, Zhang Y, Man X, Pan L, Huang Z. Experimental and modeling study on ignition delay times of dimethyl ether/n-butane blends at a pressure of 2.0 MPa. Energy Fuel 2014;28(3):2189–98.
[24] Jiang X, Zhang Y, Man X, Pan L, Huang Z. Shock tube measurements and kinetic study on ignition delay times of lean DME/n-butane blends at elevated pressures. Energy Fuel 2013;27(10):6238–46.
[25] Hu E, Pan L, Zhang Z, Huang Z. Study on ignition delay times of dimethyl ether/propane/O2/Ar mixtures at elevated pressures; 2013; 2013.
[26] Dames EE, Rosen AS, Weber BW, Gao CW, Sung CJ, Green WH. A detailed combined experimental and theoretical study on dimethyl ether/propane blended oxidation. Combust Flame 2016;168:310–30.
[27] Jiang X, Zhang Y, Pan L, Man X, Huang Z. Experimental and Modeling Study on Auto-Ignition of DME/n-Butane Blends under Engine Relevant Pressure: SAE Technical Paper; 2014. Report No.: 0148-7191.
[28] Zhang Y, Huang Z, Wei L, Zhang J, Law CK. Experimental and modeling study on ignition delays of lean mixtures of methane, hydrogen, oxygen, and argon at elevated pressures. Combust Flame 2012;159(3):918–31.
[29] Morley C. Gaseq: a chemical equilibrium program for Windows. Ver. 0.79 2005.
[30] Petersen EL, Rickard MJ, Crofton MW, Abbey ED, Traum MJ, Kalitan DM. A facility for gas-and condensed-phase measurements behind shock waves. Meas Sci Technol 2005;16(9):1716.
[31] Deng F, Yang F, Zhang P, Pan Y, Bugler J, Curran HJ, et al. Towards a kinetic understanding of the NOx promoting-effect on ignition of coalbed methane: a case study of methane/nitrogen dioxide mixtures. Fuel 2016;181:188–98.
[32] Lutz AE, Kee RJ, Miller JA. SENKIN: A FORTRAN program for predicting homogeneous gas phase chemical kinetics with sensitivity analysis: Sandia National Labs. Livermore, CA (USA): Sandia National Labs.; 1988.
[33] Kee RJ, Rupley FM, Miller JA. Chemkin-II: A Fortran chemical kinetics package for the analysis of gas-phase chemical kinetics. Livermore, CA (USA): Sandia National Labs.; 1989.
[34] Chaos M, Dryer FL. Chemical-kinetic modeling of ignition delay: considerations in interpreting shock tube data. Int J Chem Kinet 2010;42 (3):143–50.
[35] Wang Z, Zhang X, Xing L, Zhang L, Herrmann F, Moshammer K, et al. Experimental and kinetic modeling study of the low-and intermediate-

temperature oxidation of dimethyl ether. Combust Flame 2015;162(4):1113–25.
[36] Fischer SL, Dryer FL, Curran HJ. The reaction kinetics of dimethyl ether. I: High-temperature pyrolysis and oxidation in flow reactors. Int J Chem Kinet 2000;32(12):713–40.
[37] Curran HJ, Fischer SL, Dryer FL. The reaction kinetics of dimethyl ether. II: Low-temperature oxidation in flow reactors. Int J Chem Kinet 2000;32(12):741–59.
[38] Kaiser EW, Wallington TJ, Hurley MD, Platz J, Curran HJ, Pitz WJ, et al. Experimental and modeling study of premixed atmospheric-pressure dimethyl ether-air flames. J Phys Chem A 2000;104(35):8194–206.
[39] Chemical-Kinetic Mechanisms For Combustion Applications" SDMW.
[40] Li Y, Zhou C, Somers KP, Zhang K, Curran HJ. The oxidation of 2-butene: a high pressure ignition delay, kinetic modeling study and reactivity comparison with isobutene and 1-butene. Proc Combust Inst 2016.
[41] Zhou C, Li Y, O'Connor E, Somers KP, Thion S, Keesee C, et al. A comprehensive experimental and modeling study of isobutene oxidation. Combust Flame 2016;167:353–79.
[42] Burke U, Metcalfe WK, Burke SM, Heufer KA, Dagaut P, Curran HJ. A detailed chemical kinetic modeling, ignition delay time and jet-stirred reactor study of methanol oxidation. Combust Flame 2016;165:125–36.
[43] Burke SM, Burke U, Mc Donagh R, Mathieu O, Osorio I, Keesee C, et al. An experimental and modeling study of propene oxidation. Part 2: Ignition delay time and flame speed measurements. Combust Flame 2015;162(2):296–314.
[44] Burke SM, Metcalfe W, Herbinet O, Battin-Leclerc F, Haas FM, Santner J, et al. An experimental and modeling study of propene oxidation. Part 1: Speciation measurements in jet-stirred and flow reactors. Combust Flame 2014;161(11):2765–84.
[45] Metcalfe WK, Burke SM, Ahmed SS, Curran HJ. A hierarchical and comparative kinetic modeling study of C1–C2 hydrocarbon and oxygenated fuels. Int J Chem Kinet 2013;45(10):638–75.
[46] Kéromnès A, Metcalfe WK, Heufer KA, Donohoe N, Das AK, Sung C, et al. An experimental and detailed chemical kinetic modeling study of hydrogen and syngas mixture oxidation at elevated pressures. Combust Flame 2013;160(6):995–1011.
[47] Wang H, You X, Joshi AV, Davis SG, Laskin A, Egolfopoulos F, et al. USC mech version II. High-temperature combustion reaction model of H 2007;2.
[48] Williams FA. Chemical-kinetic mechanisms for combustion applications. Center for Energy Research, UCSD, http://maeweb.ucsd.edu/~combustion/cermech 2003.
[49] Zhao Z, Chaos M, Kazakov A, Dryer FL. Thermal decomposition reaction and a comprehensive kinetic model of dimethyl ether. Int J Chem Kinet 2008;40(1):1–18.
[50] Prince JC, Williams FA. A short reaction mechanism for the combustion of dimethyl-ether. Combust Flame 2015;162(10):3589–95.
[51] Smith GP, Golden DM, Frenklach M, Moriarty NW, Eiteneer B, Goldenberg M, et al. GRI-Mech 3.0. URL: http://www.me.berkeley.edu/gri_mech 1999;51:55.
[52] Wang H. A comprehensive kinetic model of ethylene and acetylene oxidation at high temperatures: University of Delaware; 1998.
[53] Laskin A, Wang H, Law CK. Detailed kinetic modeling of 1, 3-butadiene oxidation at high temperatures. Int J Chem Kinet 2000;32(10):589–614.
[54] Prince JC, Treviño C, Williams FA. A reduced reaction mechanism for the combustion of n-butane. Combust Flame 2017;175:27–33.
[55] Healy D, Kalitan DM, Aul CJ, Petersen EL, Bourque G, Curran HJ. Oxidation of C1–C5 alkane quinternary natural gas mixtures at high pressures. Energy Fuel 2010;24(3):1521–8.
[56] Tomlin AS, Agbro E, Nevrlý V, Dlabka J, Vašinek M. Evaluation of combustion mechanisms using global uncertainty and sensitivity analyses: a case study for low-temperature dimethyl ether oxidation. Int J Chem Kinet 2014;46(11):662–82.
[57] Liu D, Santner J, Togbé C, Felsmann D, Koppmann J, Lackner A, et al. Flame structure and kinetic studies of carbon dioxide-diluted dimethyl ether flames at reduced and elevated pressures. Combust Flame 2013;160(12):2654–68.
[58] Zheng XL, Lu TF, Law CK, Westbrook CK, Curran HJ. Experimental and computational study of nonpremixed ignition of dimethyl ether in counterflow. Proc Combust Inst 2005;30(1):1101–9.
[59] Goldsborough SS. A chemical kinetically based ignition delay correlation for iso-octane covering a wide range of conditions including the NTC region. Combust Flame 2009;156(6):1248–62.
[60] Campbell MF, Wang S, Goldenstein CS, Spearrin RM, Tulgestke AM, Zaczek LT, et al. Constrained reaction volume shock tube study of n-heptane oxidation: Ignition delay times and time-histories of multiple species and temperature. Proc Combust Inst 2015;35(1):231–9.
[61] Karwat DM, Wagnon SW, Wooldridge MS, Westbrook CK. Low-temperature speciation and chemical kinetic studies of n-heptane. Combust Flame 2013;160(12):2693–706.